JOURNAL OF SOLID STATE CHEMISTRY 111, 58–74 (1994)

Structures, Structural Defects, and Reactions in a Nickel Chevrel-Phase Sulfide: A High-Resolution Electron Microscope Study

Z. C. Kang and L. Eyring

Department of Chemistry and Biochemistry and Center for Solid State Science, Arizona State University, Tempe, Arizona 85287-1604

and

H. Hinode, T. Uchida, and M. Wakihara

Tokyo Institute of Technology, 2-12-1 Ookayama, Meguro-ku, Tokyo 152, Japan

Received October 18, 1993; Accepted February 18, 1994
IN HONOR OF C. N. R. RAO ON HIS 60TH BIRTHDAY

High-resolution electron microscopy is used to illuminate the structure and structural defects of the nonstoichiometric nickel Chevrel-phase sulfide $Ni_2Mo_6S_{7.6}$. The specimen consists of two phases, each showing threefold symmetry. The minor phase corresponds to that described by Guillevic *et al.* The majority phase has the same $R\bar{3}$ symmetry with $a_{hex} = 6.78$ Å and $c_{hex} = 14.5$ Å with 19 Chevrel clusters in a volume of 1732 Å^3. In extended defects such as dislocations and boundaries the clusters are preserved intact and behave as units. Electron-beam-induced decomposition does occur slowly during observation, first disordering and then reducing the clusters, yielding regions of Mo metal or Mo–Ni alloy in the edges. It has not been possible to interpret the nature of the disordered regions.

INTRODUCTION

The interesting and potentially useful chemical and physical properties of the Chevrel phases have lead to their extensive study. The purpose of this work is to apply the techniques of high-resolution electron microscopy (HREM) to explore further the structure and texture of the nickel Chevrel-phase sulfide $Ni_2Mo_6S_{7.6}$, and its electron-beam-induced decomposition. Such a study should also provide information about defects that exist in Chevrel phases. Thus far, little has been learned concerning the defects in this important family of structures.

There appears to be some ambiguity in the declared compositions of the nickel Chevrel-phase sulfides that have previously been studied. In most instances inadequate analytical data have been included in the publications to judge the accuracy of the compositions reported. Tanjo *et al.* (1) established the single-phase limits of the nickel Chevrel phase which have been recently reported by Uchida and Wakihara (2) as $Ni_{1.7-2.1}Mo_6S_{7.4-7.7}$. Outside these limits, under the conditions of their preparation, two-phase regions exist. Nevertheless, in the discussion that follows, the compositions claimed by the authors of the papers cited in each case have been recorded.

The structure of the stoichiometric Chevrel phase, $Ni_2Mo_6S_8$, has been determined by refinement of X-ray powder diffraction data by Guillevic *et al.* (3, 4). The space group is $R3$ or $R\bar{3}$. The rhombohedral unit cell parameters are $a = 6.462$ Å and $\alpha = 94.68°$. The hexagonal cell parameters are $a = 9.504$ Å and $c = 10.239$ Å. The atomic positions are as follows: Mo, $x = 0.0162$, $y = 0.1710$, $z = 0.3883$; S(1), $x = 0.3143$, $y = 0.2797$, $z = 0.4127$; S(2), $z = 0.1999$; $\frac{1}{6}$ Ni(1), $x = 0.738$, $y = 0.499$, $z = 0.318$; $\frac{1}{6}$ Ni(2), $x = 0.160$, $y = 0.246$, $z = 0.900$. More recently these same authors reported the structure of $Ni_{1.4}Mo_6S_8$ as isostructural with the stoichiometric compound and with only slightly different lattice parameters (4).

In this paper a model of the structure of $Ni_2Mo_6S_{7.6}$ is considered, using the structure of the stoichiometric compound as a reference and comparing its symmetries and atomic positions with those obtained in the specimen studied by HREM. Convergent beam electron diffraction (CBED) patterns reveal the symmetry and HREM images provide information on the positions of the atoms in real space in defect regions.

The Chevrel-phase sulfide structure consists of a nearly cubic assemblage of Mo_6S_8 clusters in which metal–metal bonded Mo atoms are at the corners of an octahedron embedded in a cube of S atoms. The Mo atoms are close to but just outside the face centers of the cube. This cluster (shown in Fig. 1a) is the basic unit in these Chevrel phases. There would be 20 electrons in the molecular orbitals of the metal–metal bonds of the mo-

0022-4596/94 $6.00

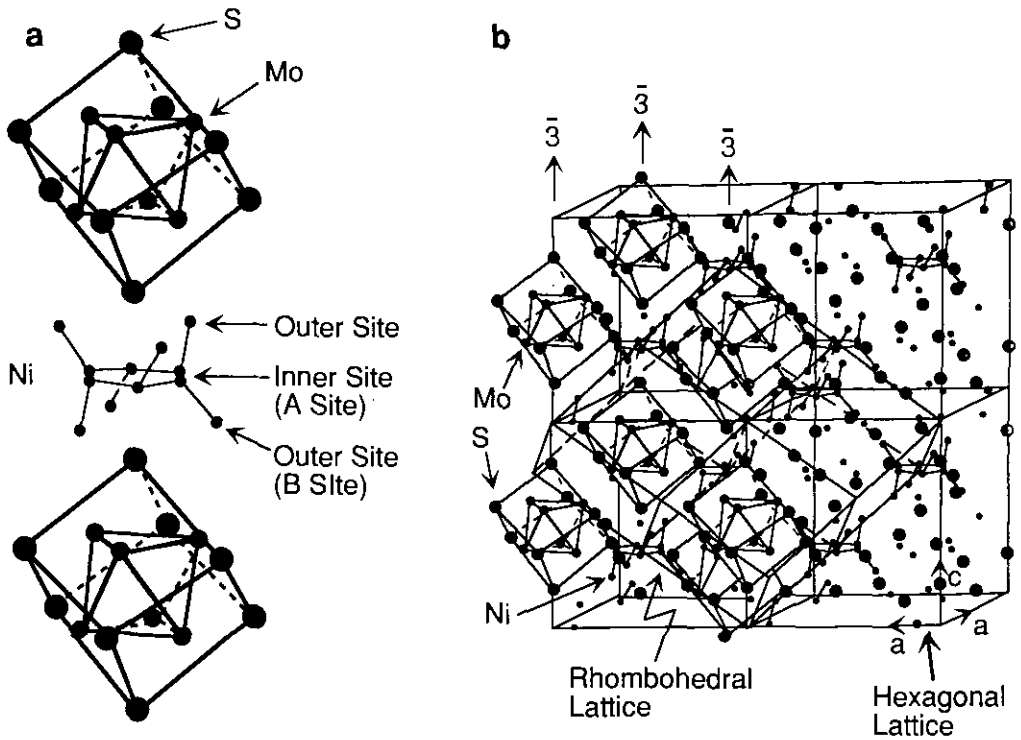

FIG. 1. (a) The basic atomic arrangements in the Chevrel cluster with respect to possible positions of the intercalated nickel atoms (after Uchida and Wakihara (2)). (b) The arrangement of the units of (a) in the nickel Chevrel-phase sulfide (after Uchida and Wakihara (2)).

lybdenum octahedron if none were contributed from some other source such as the intercalated nickel. The cubic cluster is distorted in the structure, preserving only the threefold axis. As Fig. 1b suggests, the corners of each tilted cubic cluster lie opposite the face centers of adjacent cubes forming donor–acceptor sulfur–molybdenum bonds. The nickel atoms are intercalated among the special sites (illustrated in Fig. 1) in this assemblage.

This configuration results in a rhombohedral unit cell with $\alpha \cong 90°$ and, therefore, an almost cubic shape. However, the structure would not be cubic even if α were exactly 90° since the Mo_6S_8 clusters are not oriented parallel to the unit cell vectors, but are turned by an angle of about 27° around the threefold axis (5). This means that the diffraction pattern and the high-resolution images in the threefold [0 0 1] direction will reveal important information about the structure and any structural adjustments that result from the nonstoichiometry.

EXPERIMENTAL DETAILS

The $Ni_2Mo_6S_{7.6}$ sample was prepared from a stoichiometric mixture of Ni, Mo, and S powders. The mixture was sealed in a quartz ampoule under vacuum and was heated at 1000°C for 48 hr, followed by quenching. After grinding, this procedure was repeated. Since there was no evidence of reaction of the sample with the quartz ampoule, and no trace of unreacted sulfur, the overall composition of the reactants initially sealed into the ampoule was considered to be the final equilibrium composition. Phase identification was carried out by powder X-ray diffractometry using Cu$K\alpha$ radiation (ROTAFLEX, Rigaku Denki Co., LTD). The specimen used here is clearly in the single-phase region reported by Tanjo *et al.* as shown in Fig. 2 of their paper (1).

Concerning the basis of nonstoichiometry of Chevrel-phase sulfides, Wada *et al.* (6) measured the density to determine the defect type in the iron Chevrel-phase sulfides. The measured density is in good agreement with the value calculated from a sulfur vacancy model. This work supports our assumption that the nickel Chevrel phase also has sulfur vacancies. However, the concentration of vacancies is small ((8–7.6)/8 = 0.05) and probably not detectable in HREM.

The powdered product, sonicated in pure alcohol, was captured on holey carbon grids for observation in the JOEL 2000FX and 4000EX electron microscopes operated at 200 and 400 kV, respectively. A video recording of the slow *in-situ* decomposition of the Chevrel-phase sulfide was made during observation in the JEOL 4000EX electron microscope.

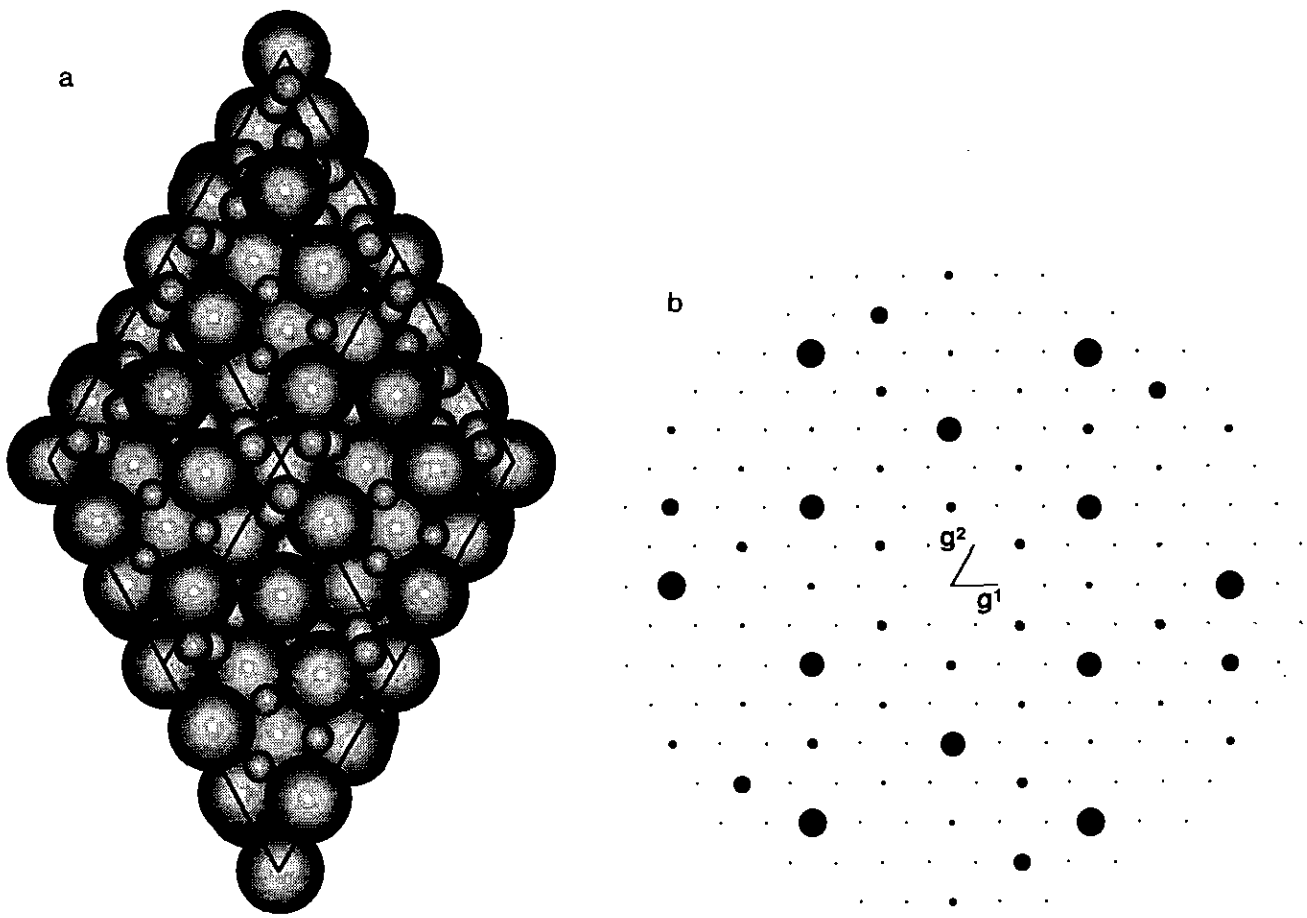

FIG. 2. (a) The atomic arrangement of the Chevrel phase in the [0 0 0 1] projection (from data in Refs. (3, 4)). (b) The calculated diffraction pattern of the Chevrel phase in the [0 0 0 1] projection.

RESULTS AND DISCUSSION

Figure 2a shows the atomic arrangement of the Chevrel phase in the [0 0 0 1] projection. The calculated kinematic diffraction pattern from this projection is shown in Fig. 2b. The electron microscope images calculated using the multislice method, as a function of specimen thickness and microscope defocus (7), are shown in Fig. 3a. Some experimental images are shown in Fig. 3b. Note that the black-dot image **a** corresponds to a defocus of approximately −500 Å corresponding to the first Scherzer defocus. The white-dot image **c** corresponds to the second Scherzer defocus at about 760 Å, while the image **b** indicates a defocus of about 600 Å. In anticipation of the need to compare the diffraction patterns and images of the Chevrel phase in another zone they are calculated (see Fig. 4) along the [1 1 $\bar{2}$ 1] direction of the hexagonal cell. (This would be the [1 0 0] direction of the cubic cell if it were not distorted.)

The kinematic diffraction pattern calculated for $Ni_2Mo_6S_8$ from the structural data given by Guillevic *et al.* (3, 4) is shown in Fig. 2b. It indicates the arrangement of the Mo atoms by the strongest spots because the metal atoms have larger scattering factors. The *d*-spacing corresponds to one-half the distance between the Mo atoms. The weakest spots indicate the unit cell. Figure 5 is the experimental diffraction pattern of one region of the sample. It is similar to that calculated and shown in Fig. 2b. More frequently, however, the diffraction pattern shown in Fig. 6 is observed. Both structures have threefold symmetry, but the very weak spots in the former are missing in the latter. This indicates that the unit cell of the major phase is smaller than that of the minor phase. Furthermore, the unit cell vectors are rotated by 30°.

In order to establish the true symmetry of this majority phase, convergent beam diffraction patterns were taken (8). Figure 7a shows the CBED pattern for the zero-layer Laue zone. This pattern demonstrates the threefold sym-

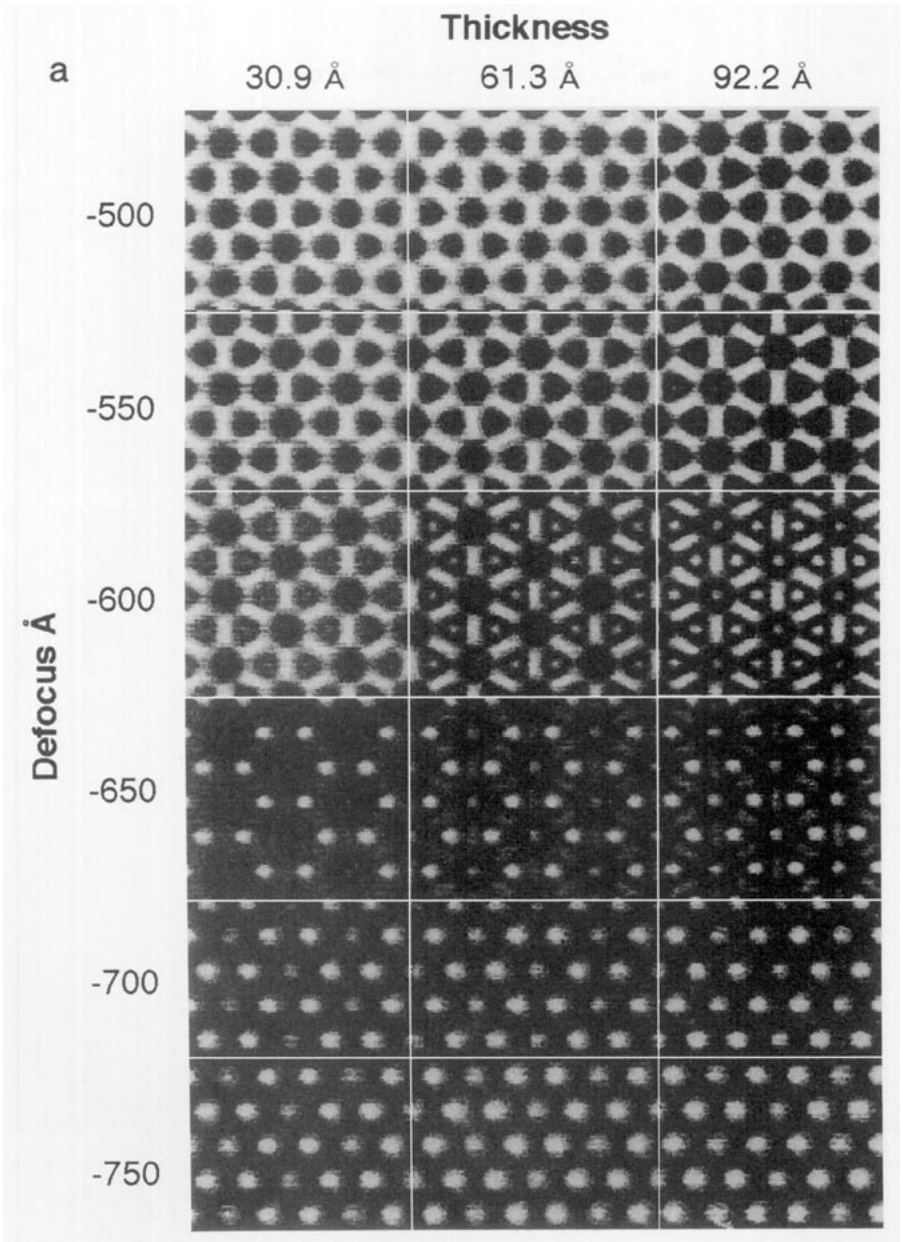

FIG. 3. (a) Calculated multislice images of the Chevrel phase as a function of specimen thickness and microscope defocus. (b) The experimental images to be compared with (a). Note the evolution from black-dot to white-dot condition from a to c.

metry in the central and all other discs. The higher order Laue zone (HOLZ) pattern shown in Fig. 7b confirms the threefold symmetry of the whole pattern. The CBED pattern of the [1 1 $\bar{2}$ 1] zone of the hexagonal structure reproduced in Fig. 7c shows no fourfold symmetry such as would be necessary if cubic symmetry were present. The experimental diffraction pattern in this zone (Fig. 7d) should be compared with that calculated for the reported stoichiometric compound recorded in Fig. 4. These results indicate that removal of the sulfur does not change the space group, $R\bar{3}$ (3, 4). The unit cell of the majority phase has a_{hex} = 6.78 Å and c_{hex} = 14.5 Å and contains 19 Mo_6S_8 clusters in a volume of 1732 Å^3. This suggests that there are nine or more vacant sulfur sites per unit cell. This would require random occupancy of the sulfur atom positions since the threefold axis is present.

In order to image the cluster arrangement directly this crystal is best viewed down the [0 0 0 1] zone axis. Figure 8a is such an image and the inset confirms that the

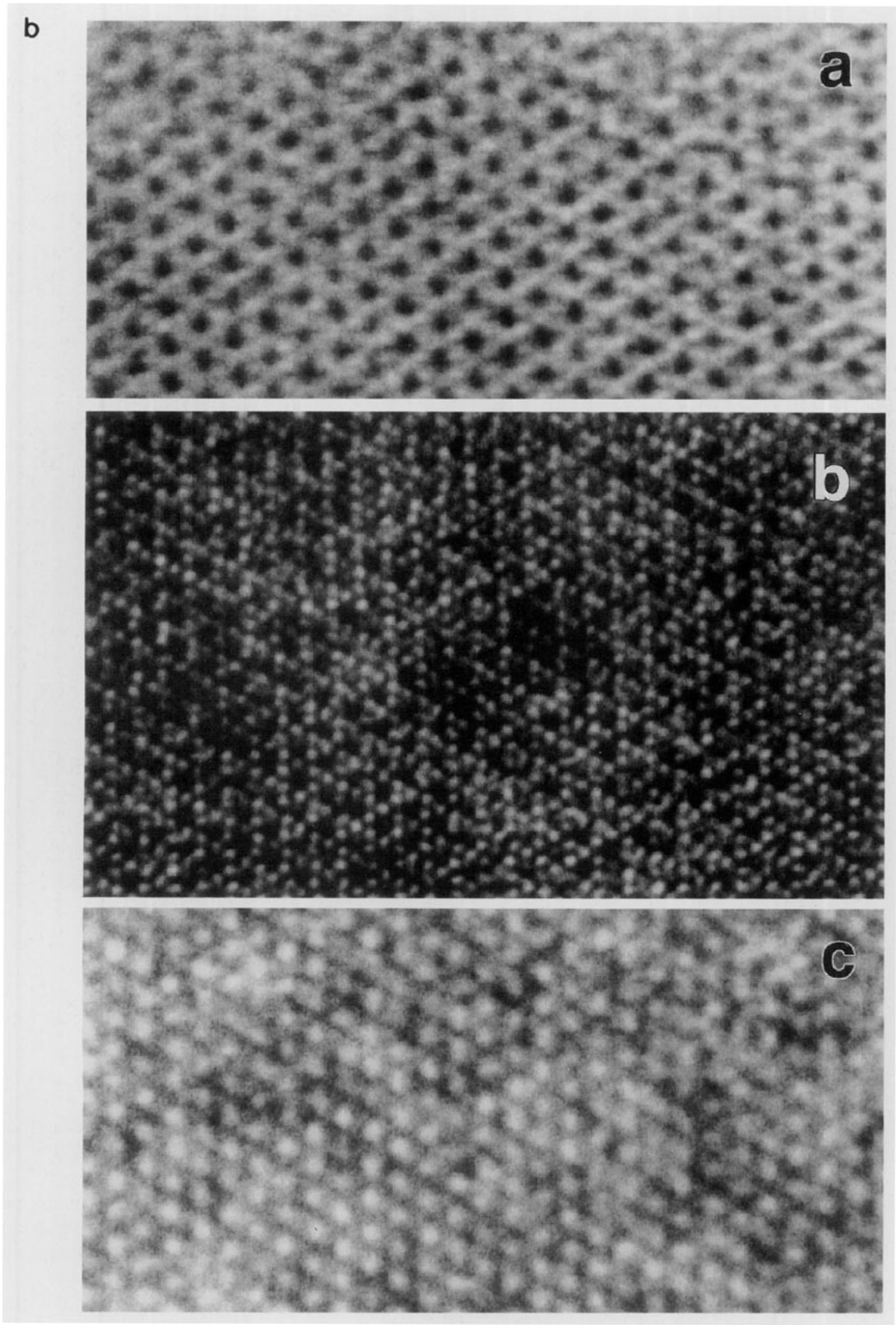

FIGURE 3—*Continued*

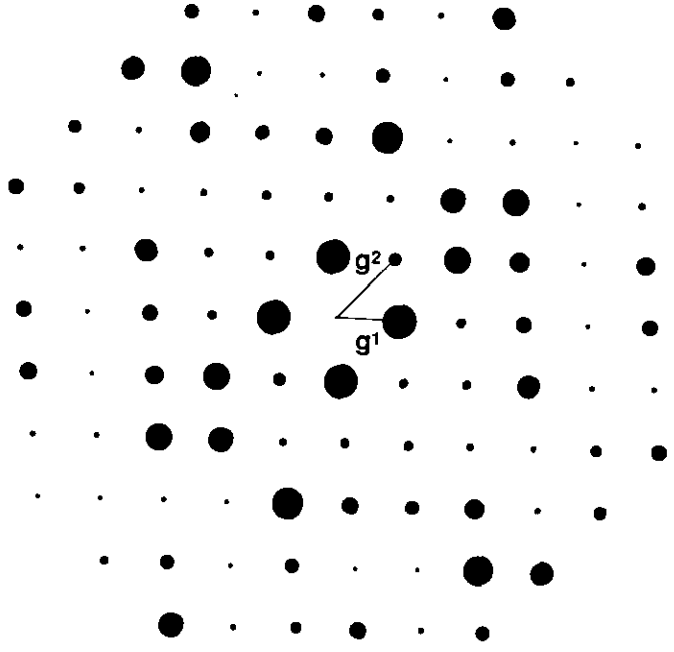

FIG. 4. The calculated electron diffraction pattern of the Chevrel phase along the [1 1 $\bar{2}$ 1] direction of the hexagonal cell.

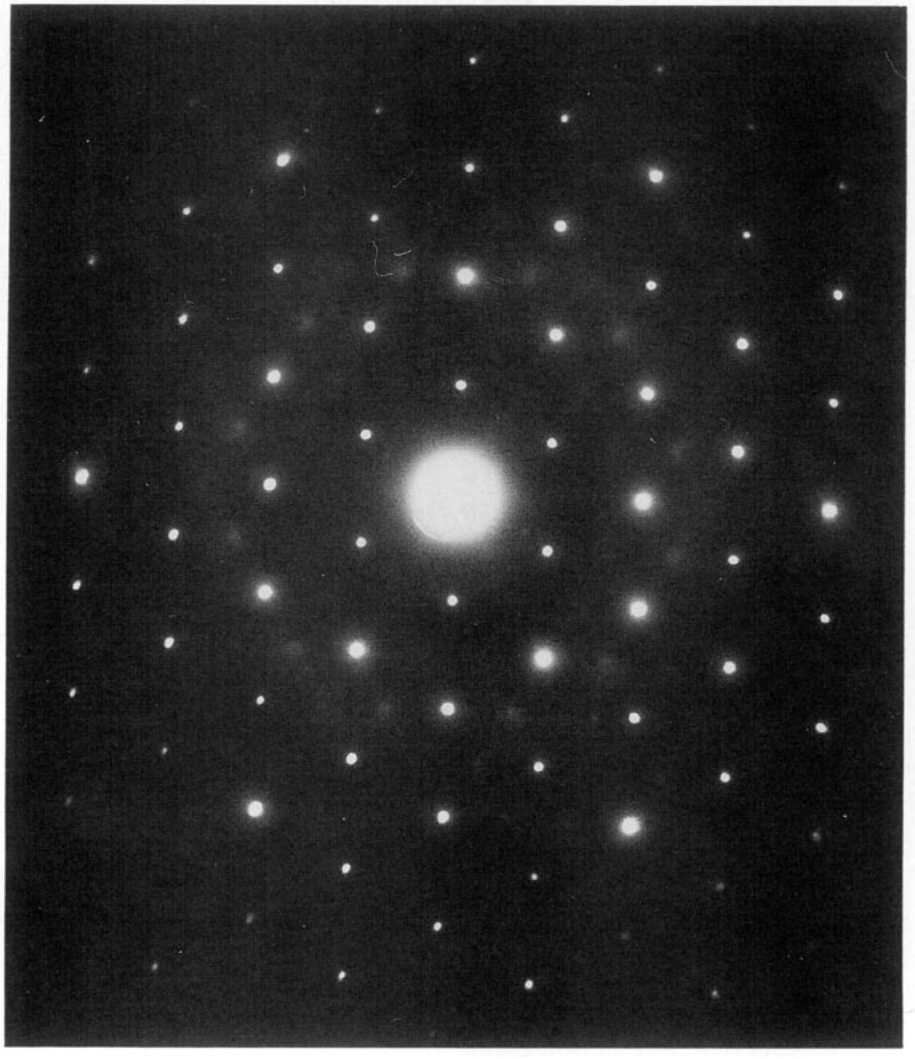

FIG. 5. An observed diffraction pattern to be compared with the calculated pattern shown in Fig. 2b.

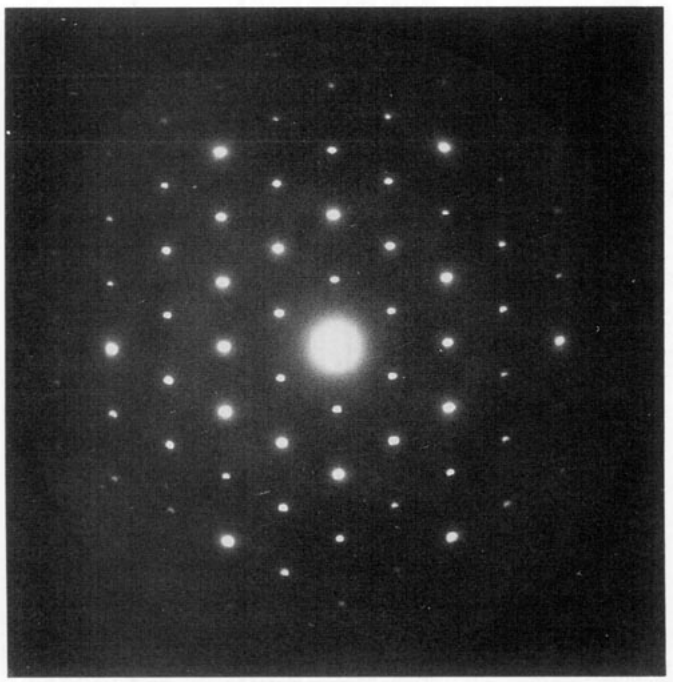

FIG. 6. The most commonly observed diffraction pattern. Note the absence of the weak reflections of Fig. 5.

cluster arrangement corresponds to that of the published structure of the stoichiometric material. This imaged region of the crystal has many imperfections but the overall arrangement of the clusters is clear. It should be noted by comparison with Fig. 3a that the observed and calculated images are very similar. Although the images of the clusters vary as they must, if some have sulfur deficiencies, it is not obvious that the sulfur atom deficits are regularly arranged.

Figure 8b presents the high-resolution image of $Ni_2Mo_6S_{7.6}$ in the [1 1 $\bar{2}$ 1] zone. The inserted sketch shows the cluster arrangement in this zone. Again, there appear to be no symmetry differences between the two structures observed in the specimen and that published as the structure for the stoichiometric nickel Chevrel phase.

EXTENDED DEFECTS OBSERVED IN THE NICKEL CHEVREL PHASES

Defects in metals, alloys, semiconductors, and any ordered materials where the interparticle bonding is at the atomic level have been extensively studied, some exhaustively. However, little information has appeared about defects in aggregations of greater complexity such as in cluster compounds where the elementary particles consist of several atoms. This HREM study of the nickel Chevrel phases has yielded a view of some types of extended defects that exist in the original material and in beam-induced decomposition products.

A. An "Edge" Dislocation

Figures 9a and 9b are a $[1\ 1\ \bar{2}\ 1]_{hex}$ zone image of a region of the original crystalline Chevrel phase in which an edge dislocation can be clearly seen. This region is shown in the white-dot condition in Fig. 9a and near the black-dot condition in Fig. 9b. In each image a single Mo_6S_8 cluster is the complex white or black blob making up the pattern. The dislocation can be easily observed in either, but is more clearly seen in Fig. 9b.

If we choose the cluster as the ultimate element of the structure and make a Burgers circuit around the dislocation core in the regular structure, we obtain the Burgers vector, $[1\ 0\ 1\ 1]_{hex}$. (This would be the $[0\ 1\ 0]_{cub}$ direction if it actually had that symmetry.) There is only one extra plane of clusters inserted into the regular structure.

The small distortion of the region is centered about the core of the dislocation. The clusters at the core of the dislocation are apparently rotated, and accommodation has been made for some extra nickel atoms if stoichiometry is preserved. The core image in Fig. 9b suggests that an additional nickel atom could be located in the extra tunnel formed by the five Mo_6S_8 clusters at the core of the dislocation to preserve charge balance.

There is a group of dislocations located in the same plane that create great distortions (Fig. 9c). The positive and negative "edge" dislocations balance the charge, but two dislocations of the same sign create a large strain.

b. Interfaces

An interface in the nickel Chevrel phase can be either coherent or incoherent. The different types that have been observed are shown in Fig. 10. A coherent tilt boundary in which dislocations occur at regular intervals is shown in Fig. 10a. Figure 10b records a shear displacement coherence boundary, but the extra planes of dislocations are almost perpendicular to the boundary and cause the observed distortion. A boundary caused by an irregular arrangement of dislocations is shown in Fig. 10c.

c. Decomposition Processes

Little has thus far been said of the mechanisms of formation or decomposition of the Chevrel phases. These HREM studies provide an opportunity to observe the *in situ* electron-beam-induced decomposition of the nickel Chevrel phase. This capability depends on the time-resolved recording of the changes occurring at essentially

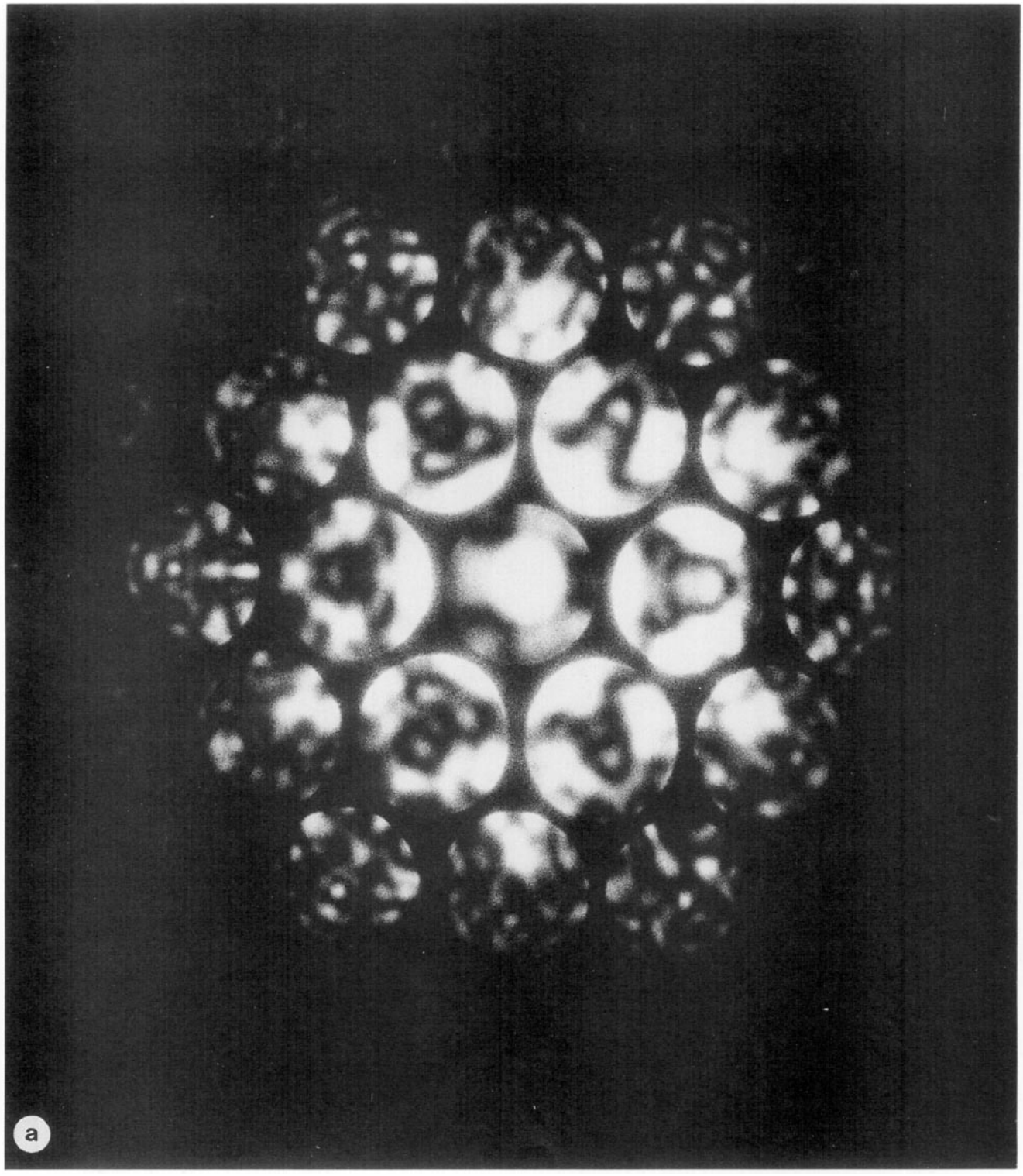

FIG. 7. (a) A CBED diffraction pattern for the zero-layer Laue zone of the Chevrel phase showing the threefold symmetry. (b) A higher order Laue zone confirming the threefold symmetry. (c) A CBED pattern in the [1 1 $\bar{2}$ 1] zone showing the absence of fourfold symmetry. (d) A diffraction pattern in the [1 1 $\bar{2}$ 1] zone to be compared to that shown in Fig. 4.

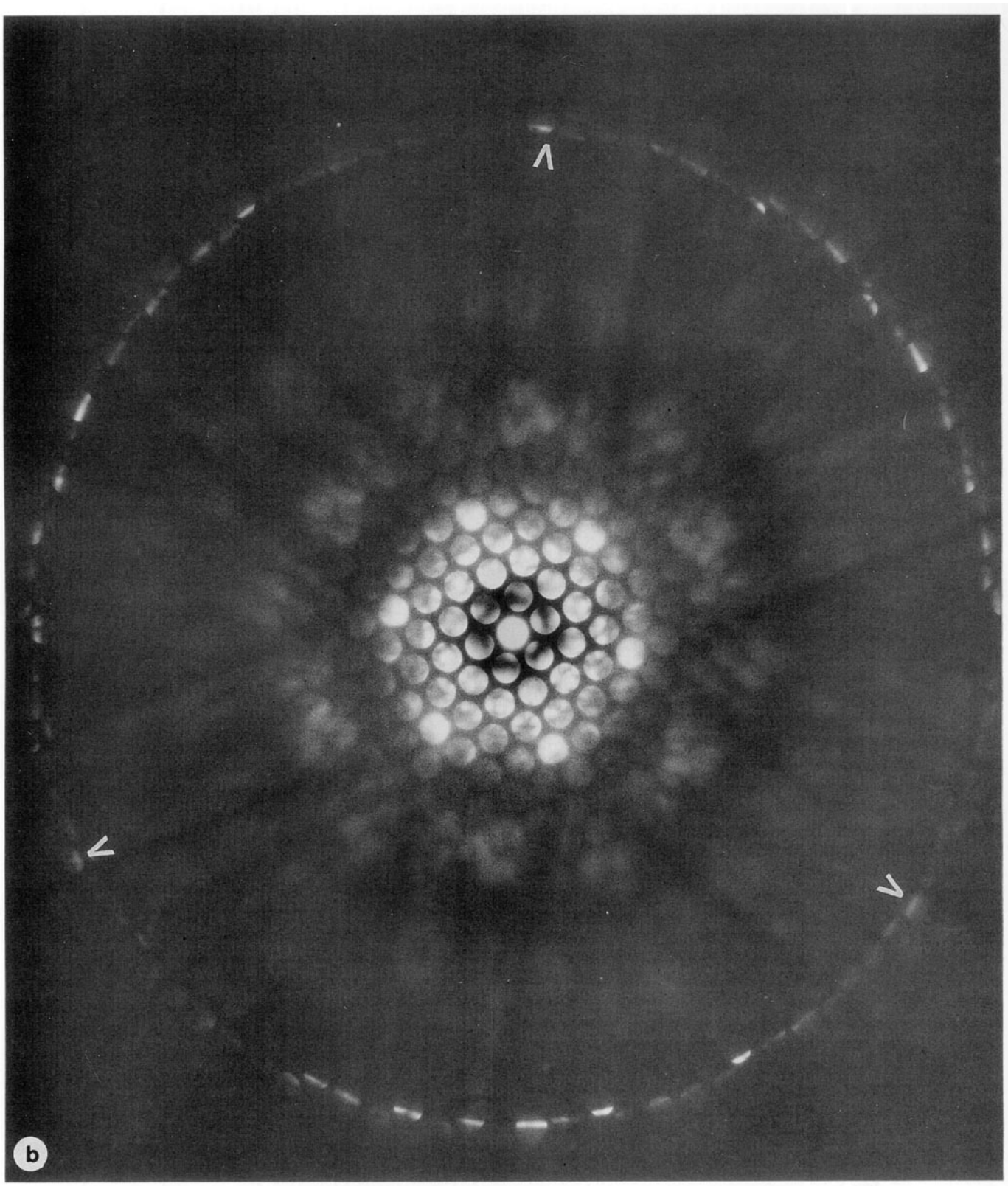

FIGURE 7—*Continued*

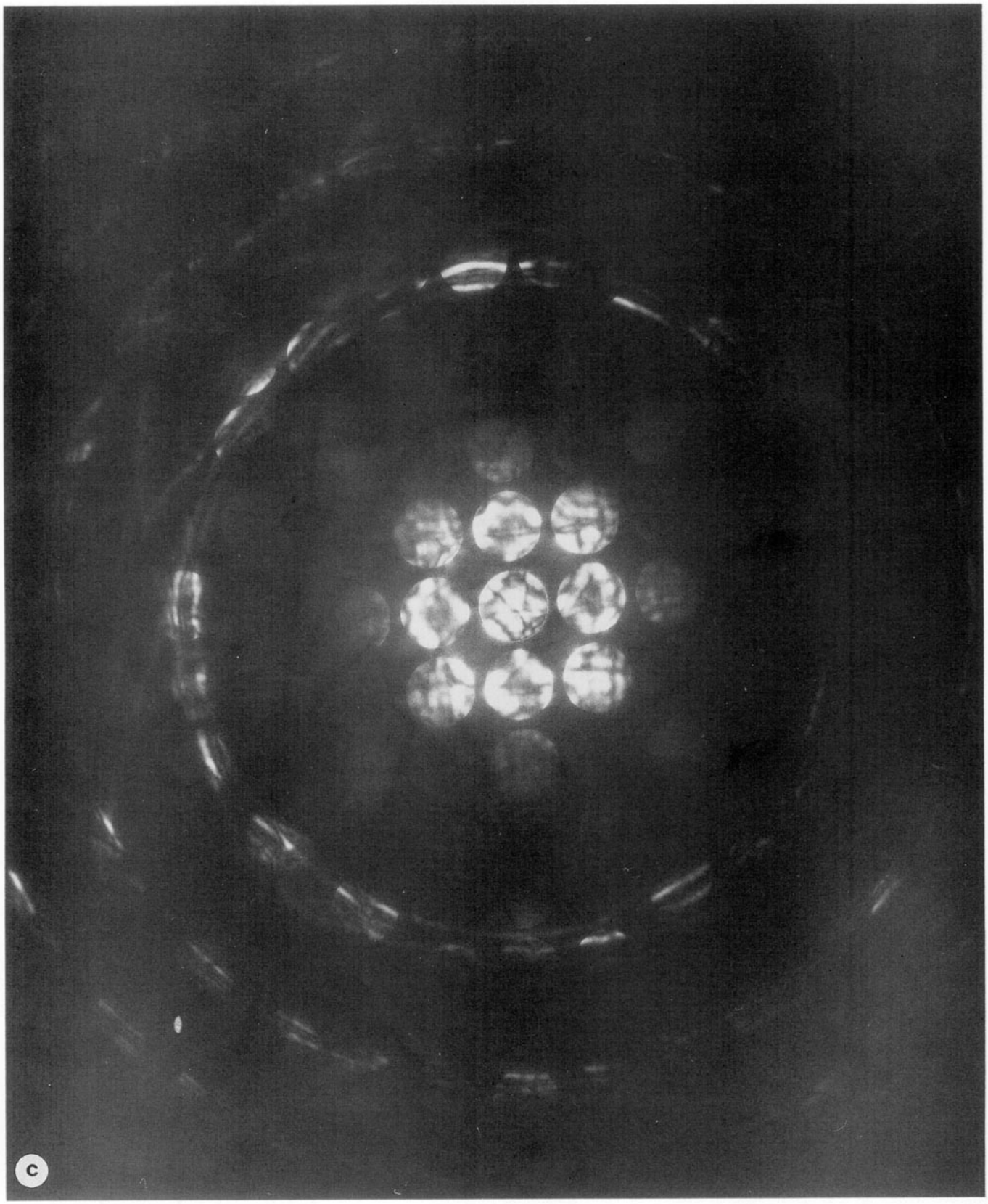

FIGURE 7—*Continued*

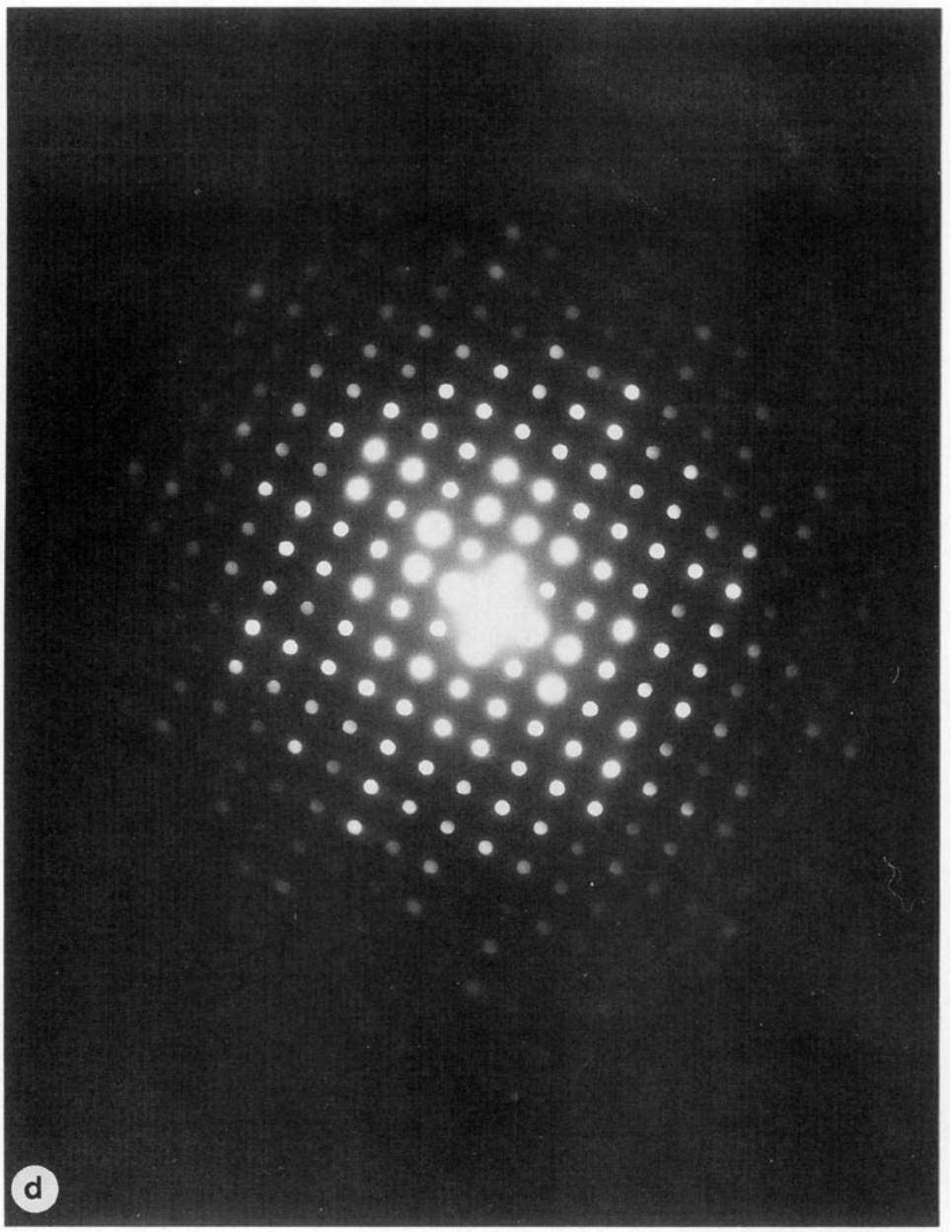

FIGURE 7—*Continued*

atomic resolution in the specimen during observation in the electron microscope. Shown in Fig. 11 are micrographic records of these changes occurring over scores of minutes. Figure 11a shows the specimen before much decomposition has occurred. The structure of the specimen can be identified by reference to Figs. 3a and 8a. The clusters may be considered to be the dark, irregular spots forming an almost hexagonal net. At this stage the regular structure persists almost to the edge. Twenty minutes later the image in Fig. 11b was recorded and extensive changes are manifest. In the thicker regions the image is not greatly changed, but in the intermediate regions increasing disorder is apparent and at the edge new structure types are indicated by fringes of about 2.4 Å spacing. Figure 11c, recorded 1 hr later, shows the distinct advance of the decomposition processes. The obvious candidates for reaction products would be Mo, Ni, nickel sulfides, and molybdenum sulfides. Analysis of the image indicates that some areas are Mo or a dilute Mo–Ni alloy.

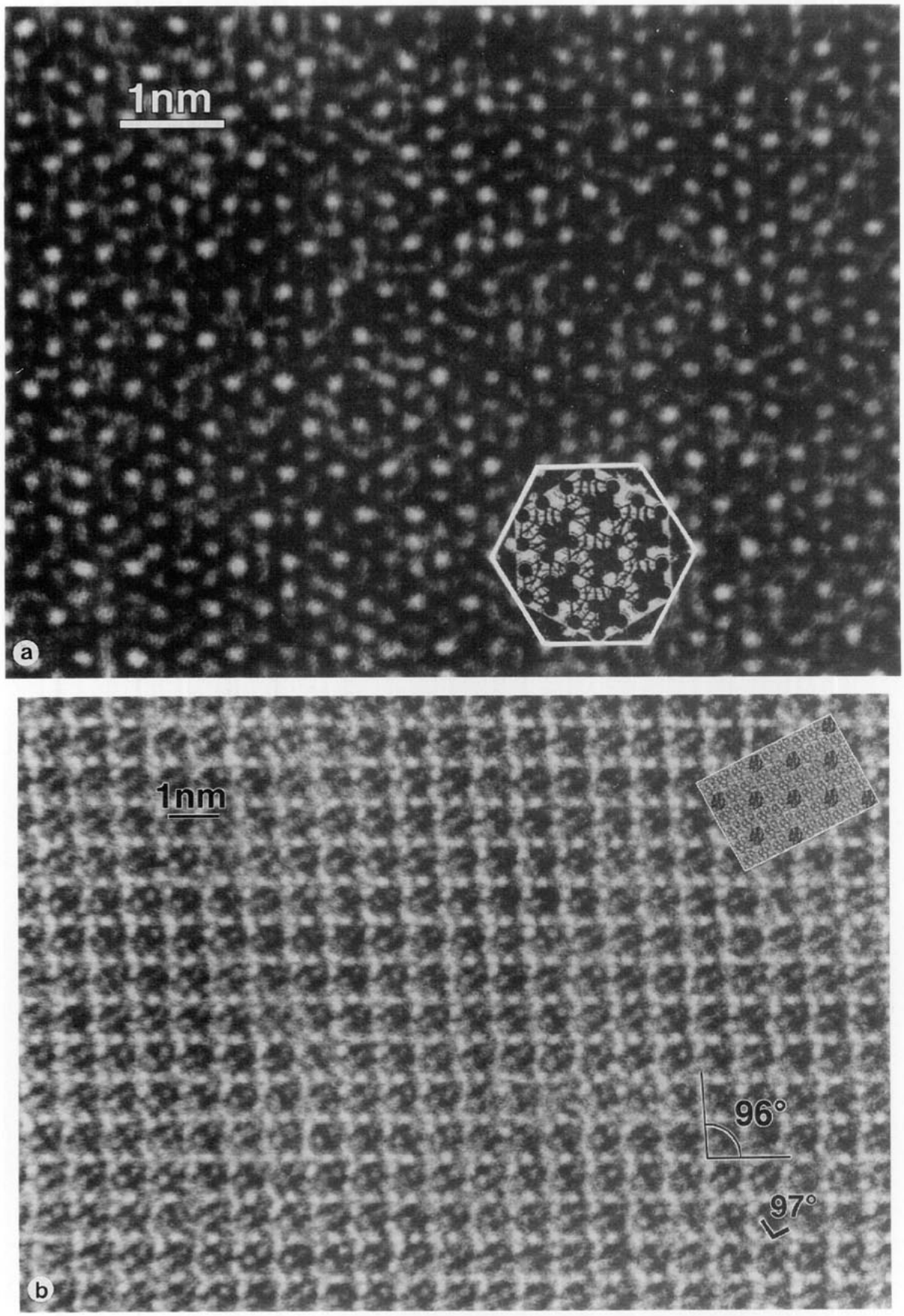

FIG. 8. (a) The experimental image taken down [0 0 0 1] with an inserted structural model. (b) The observed high-resolution image down [1 1 $\bar{2}$ 1] with a drawn image model inserted.

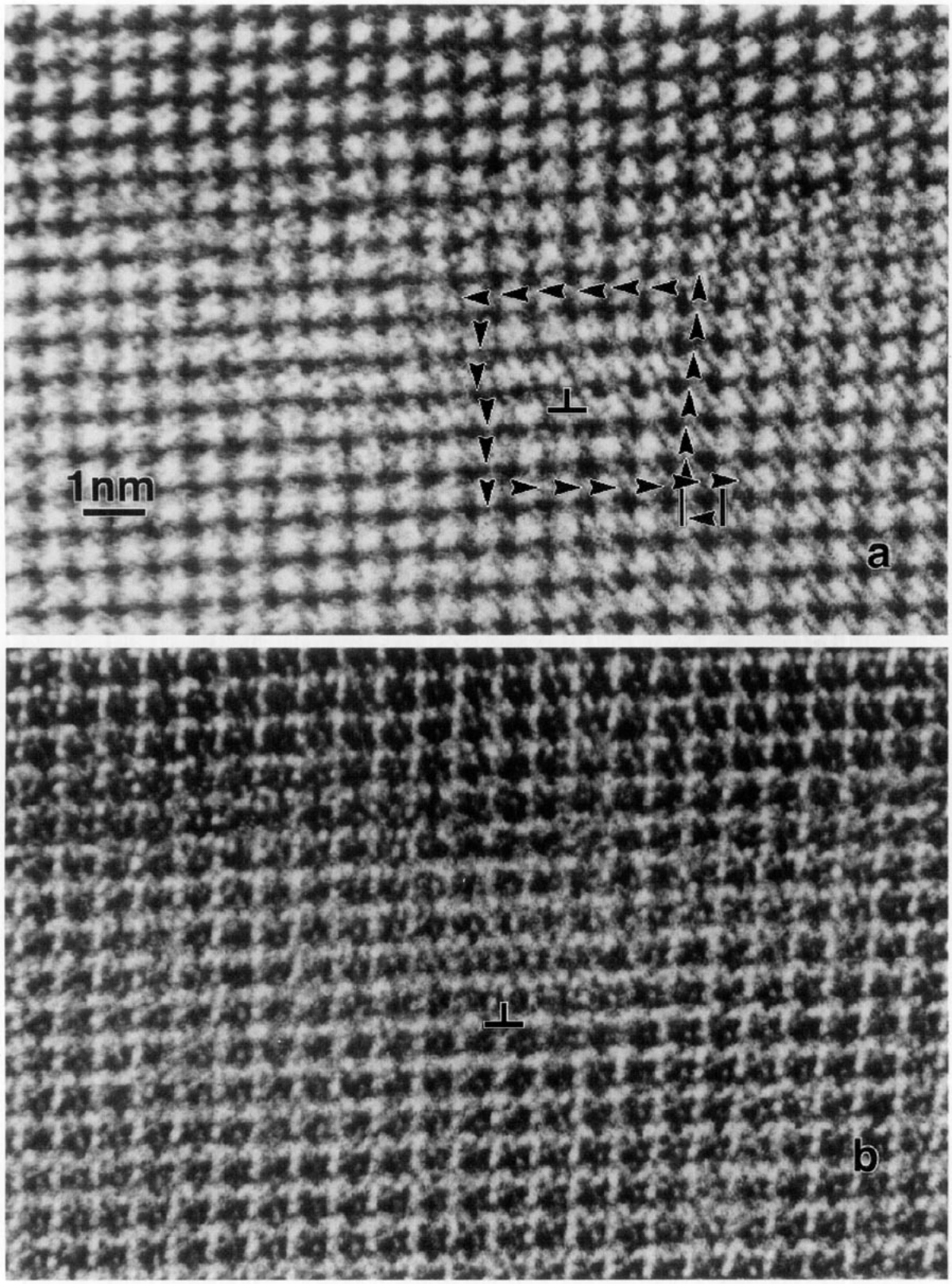

FIG. 9. (a) A [1 1 $\bar{2}$ 1] zone image of the Chevrel phase in the white-dot condition showing an edge dislocation. (b) The same region as shown in (a) in the black-dot condition. (c) A highly distorted region of the crystal resulting from a group of dislocations.

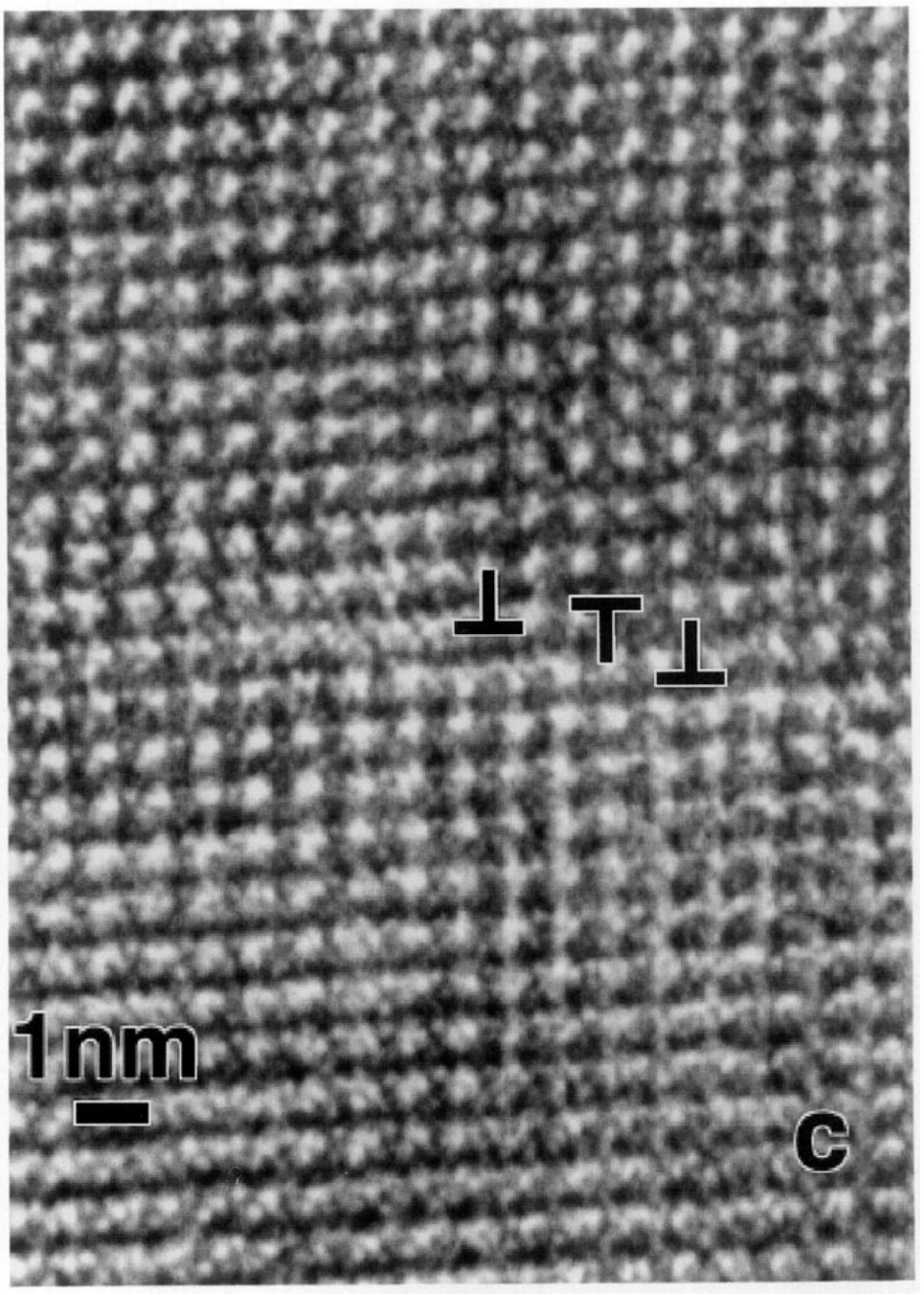

FIGURE 9—*Continued*

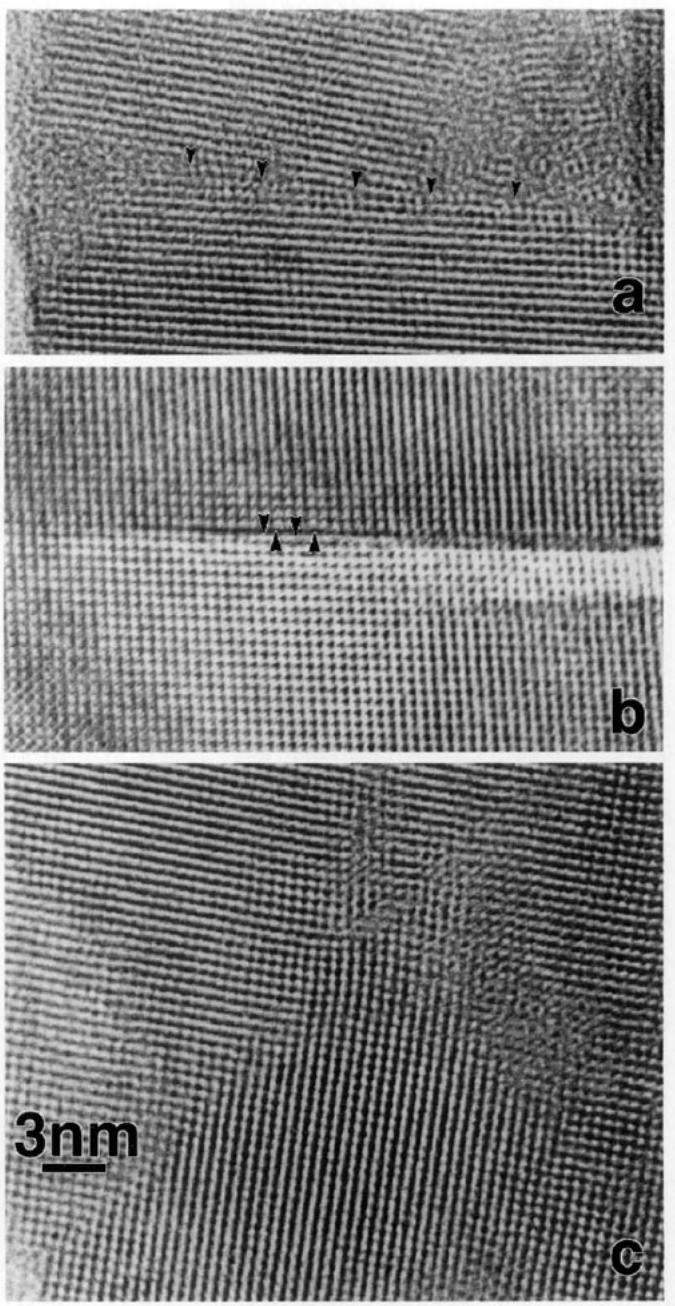

FIG. 10. Various boundaries observed in the Chevrel phase. (a) A coherent tilt boundary. (b) A shear displacement coherence boundary. (c) A boundary resulting from an irregular arrangement of dislocations.

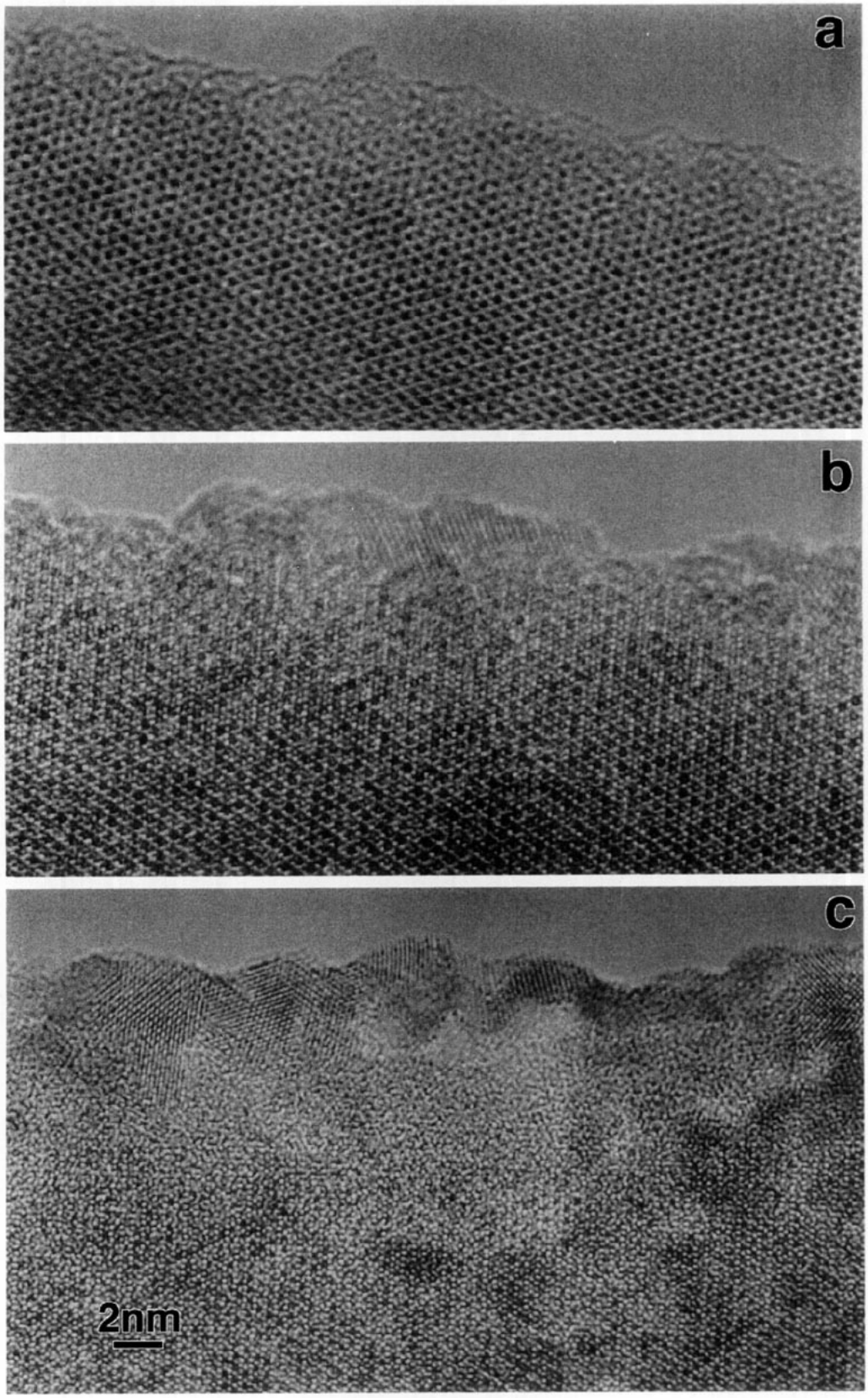

FIG. 11. Images showing the progress of beam-induced decomposition of the Chevrel phase over about 80 min. irradiation. (a) A region relatively free of decomposition. (b) The same region of the crystal about 20 min later showing substantial decomposition. (c) One hour later the details of the decomposition are clearly shown. There is a disordered region separating the undecomposed crystal from the ordered decomposition products at the edge.

ACKNOWLEDGMENTS

It is a pleasure to credit Y. Tanjo with preparation of the specimen studied and the National Science Foundation for Research Grant DMR-9114799 and Grant DMR-9115680 in support of the HREM facility at Arizona State University.

REFERENCES

1. Y. Tanjo, T. Uchida, and M. Wakihara, *Denjki Kagaku* **57,** 553 (1989).
2. T. Uchida and M. Wakihara, *Thermochim. Acta* **174,** 201 (1991).
3. J. Guillevic, O. Bars, and D. Grandjean, *J. Solid State Chem.* **7,** 158 (1973).
4. J. Guillevic, O. Bars, and D. Grandjean, *Acta Crystallogr. Sect. B* **32,** 1338 (1976).
5. K. Yvon, *in* "Current Topics in Materials Science" (E. Kaldis, Ed.), p. 55. North-Holland, Amsterdam (1979).
6. H. Wada, M. Onoda, N. Nozaki, and I. Kawada, *J. Less-Common Met.* **113,** 53 (1985).
7. J. M. Cowley, *in* "Diffraction Physics." North-Holland/American Elsevier, Amsterdam (1975).
8. J. W. Steeds, *in* "Introduction to Analytical Electron Microscopy" (J. J. Hren, J. I. Goldstein, and D. C. Joy, Eds.), p. 387. Plenum, New York (1979).